



Importance of constructing synergistic protective layers in Si-reduced graphene oxide-amorphous carbon ternary composite as anode for lithium-ion batteries

Yang Yang, Guiyan Sun, Jiali Lin, Dingqiong Chen, Yiyong Zhang, Jinbao Zhao*

State Key Laboratory of Physical Chemistry of Solid Surfaces, College of Chemistry and Chemical Engineering, Collaborative Innovation Center of Chemistry for Energy Materials, Xiamen University, Xiamen 361005, China



ARTICLE INFO

Article history:

Received 8 April 2017

Received in revised form

4 June 2017

Accepted 5 June 2017

Available online 6 June 2017

Keywords:

Si

Lithium-ion battery

Anode

Reduced graphene oxide

Synergistic protective layers

ABSTRACT

Si is regarded as a promising anode candidate for lithium-ion batteries (LIBs) due to its high theoretical capacity and appropriate Li⁺ ions insertion voltage (<0.4 V vs Li⁺/Li). However, its intrinsic inferior electronic conductivity and huge volume changes during cycling lead to poor cyclic performance. Integrating Si with carbon materials has been proved to be an efficient route to improve its electrochemical performance. In this report, we successfully synthesized Si-reduced graphene oxide-amorphous carbon (Si-rGO-C) composite assisted with a facile guar gum hydrogel method and studied the protective effect of different kinds of carbon. In the Si-rGO-C ternary composite, the Si nanoparticles (NPs) are embedded in amorphous carbon and tightly anchored to rGO sheets. The amorphous carbon and rGO serve as synergistic protective layers. The Si-rGO-C composite possesses good structural integrity accompanied by enhanced conductive framework. The resulting Si-rGO-C composite exhibits much improved electrochemical performance (a high capacity of 913 mAh g⁻¹ can be maintained after 100 cycles at 0.5 A g⁻¹ with almost no capacity decay) compared with the Si-rGO and Si-C composites with only single protective layer, indicating the importance of constructing synergistic carbon layers in Si-rGO-C ternary composite for LIB anodes.

© 2017 Elsevier B.V. All rights reserved.

1. Introduction

Since the successful commercial launch of lithium ion batteries (LIBs) by Sony Corporation 26 years ago (1991), LIBs have been extensively utilized for the present-day portable electronic devices [1,2]. However, there is a crucial demand to develop LIBs with higher energy density with the growing need for electric vehicle and energy storage system [3,4]. Anode is an indispensable component of LIB, increasing the specific capacity of anodes is an effective approach to increase the energy density of LIB. Nowadays the widely used LIB anode is still graphite, but its theoretical capacity is only 372 mAh g⁻¹ [5,6]. Thus developing anode materials having much higher capacity to replace graphite is a direct approach to boost the LIB energy density [7].

Si is considered to be one of the most promising anode candidates on account of its high theoretical specific capacity (4200 mAh

g⁻¹) and appropriate Li⁺ ions insertion potential (<0.4 V vs Li⁺/Li) [8–10]. However, Si is easy to pulverize due to huge volume changes (~300%) during repeating Li insertion and extraction processes, combined with its intrinsically low electronic conductivity, the capacity of Si anodes decays quickly [11,12].

Many efforts have been made to overcome these challenging obstacles. One effective way is to fabricate nanostructured or nanoscale Si anodes such as Si nanoparticle [13,14], Si nanowire [15–17], Si nanotube [18,19], Si thin film [20,21] and hollow Si [22–24]. These nanoscale morphologies are designed to provide facile strain relaxation to minimize electrode pulverization and shorten the diffusion paths of Li⁺ ions [25,26]. Another feasible route is to integrate Si with an electronically conducting carbon matrix [27–32]. Recently, graphene has been extensively studied to construct the conducting networks between Si because of its good mechanical flexibility and high electronic conductivity [31,33–35]. The graphene sheets can not only enhance the electronic conductivity but also work as a protective layer to relieve the strain during cycling [36]. How to make Si particles tightly anchored to the graphene sheets is the key point. Zhong et al. [32] fabricated sandwich-like graphene-Si hybrid films

* Corresponding author.

E-mail address: jbzhao@xmu.edu.cn (J. Zhao).

by hydrothermal process and electrostatic adsorption. Lin et al. [33] synthesized Si@carbon/rGO composite assisted by polyaniline. Chang et al. [34] prepared carbon-coated Si/rGO nanostructure anchored by nickel foam with carbon nanotubes by chemical vapor deposition (CVD) method. Lin et al. [35] prepared yolk-shell Si-rGO/amorphous carbon material by means of electrostatic self-assembly and hydrothermal process. All of these studies indicated that constructing dual-carbon layers (amorphous carbon and graphene) to fabricate Si-rGO-C ternary composite can greatly improve cycle performance of Si-based anodes. However, these synthetic processes usually involve hydrothermal method, CVD or HF etching, which is costly and complex. It is still a challenge to develop a simple and scalable route to fabricate Si-rGO-C ternary composite with superior electrochemical performance.

Herein, we report a facile and effective strategy for synthesis of Si-rGO-C ternary composite. All of the raw materials are commercially available and without treatment, and the process is simple and scalable. First, the Si NPs, GO and guar gum are added into water, after stirring a hydrogel is formed (Fig. 1). Then, the hydrogel is freeze-dried and annealed in inert gas to obtain the final Si-rGO-C composite. The guar gum not only helps to form hydrogel in which Si and GO are glued together but also serves as carbon source which can be carbonized to amorphous carbon after pyrolysis. In this specific structure, the Si NPs coated with amorphous carbon are well wrapped by rGO to maintain the good structural integrity and conductive contact. In order to study the importance of constructing these synergistic protective layers (amorphous carbon and graphene), the Si-C (without GO added) and Si-rGO (without guar gum) samples are also prepared according to the same method. The Si-rGO-C composite exhibits the best electrochemical performance compared to Si-C and Si-G samples.

2. Experiment

2.1. Chemicals and materials

The Si NPs powder (crystalline, APS \leq 50 nm, 98%, Alfa aesar), GO aqueous suspension (wt% = 2%, Shanghai Ashine Technology Development Co., Ltd), and guar gum (Henan Honest Food Co., Ltd) were used as received without further purification.

2.2. Synthesis of Si-rGO-C ternary composite

In a typical synthesis, 2 g GO aqueous suspension was added into 8 mL of deionized water and dispersed by ultrasonication for 1 h. 0.1 g Si NPs powder were added into 10 mL deionized water and dispersed by ultrasonication for 1 h. The Si NPs aqueous dispersion was mixed with the as-obtained GO aqueous dispersion, 0.3 g guar gum was added and stirred vigorously for 3 h. The resulting hydrogel was freeze-dried and annealed at 700 °C for 3 h under a H₂/Ar (v/v = 10: 90) atmosphere with the heat rate of 5 °C min⁻¹ to obtain the final Si-rGO-C ternary composite. The Si-rGO and Si-C composites were prepared by the same procedure without the addition of guar gum and GO, respectively.

2.3. Characterization

X-ray diffraction (XRD) patterns were collected with a Rigaku miniflex 600 instrument using Cu K α radiation ($\lambda = 0.154$ nm). Raman spectrum were measured using the inVia Raman microscope (Renishaw) equipped with a 532 nm Ar-ion laser. Material morphology was visualized by using a field-emission scanning electron microscopy (FE-SEM, Hitachi S4800). TEM images were obtained on the high-resolution transmission electron microscopy (HR-TEM, FEI, TECNAI G2 F30) and (JEOL-2100). Thermogravimetric

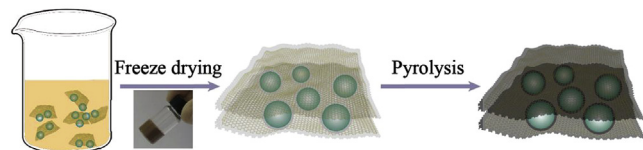


Fig. 1. Schematic synthesis process for the Si-rGO-C ternary composite.

analysis (TGA) was conducted on the SDT Q600 (TA Instruments) under air flow (20–800 °C with the heat rate of 10 °C min⁻¹). Powder electronic conductivity measurements were conducted on the Power Resistivity Meter SZT-D (Suzhou Jingge Electronics Co., Ltd.).

2.4. Electrochemical measurements

The working electrode was fabricated by mixing 60 wt% composite, 20% acetylene black, 10% vapor grown carbon fiber (VGCF), and 10% bi-component binders of same weight ratio of carboxyl methyl cellulose (CMC) and styrene-butadiene resin (SBR) in deionized water into a homogenous slurry. The slurry was coated onto a Cu foil and then dried in a vacuum oven at 80 °C for 12 h. The loading weight was 1.1–1.4 mg cm⁻². All specific capacities in the manuscript were calculated based on the total mass of the active material (including Si, amorphous carbon, and reduced graphene oxide). The 2016-type coin cells were assembled by using lithium metal as the counter electrode and celgard 2400 as the separator. The electrolyte was LiPF₆ (1 M) in the mixture of ethylene carbonate (EC)/diethyl carbonate (DEC) (v/v = 1: 1) containing 10 wt% fluoroethylene carbonate (FEC) as the additive. The charge-discharge experiments were carried out on a battery cycler (Neware BTS battery charger, Shenzhen, China) at various current rates. Electrochemical impedance spectroscopy (EIS) measurements were performed on the Autolab 302N with the frequency range from 0.1 Hz to 100 kHz. Cyclic voltammetry (CV) tests were carried out on the CHI 1030C electrochemical workstation at the scan rate of 0.1 mV s⁻¹. All of the electrochemical properties were measured at 25 °C.

3. Results and discussion

The X-ray diffraction (XRD) patterns of pristine Si, Si-rGO, Si-C and Si-rGO-C samples are shown in Fig. 2. Diffraction peaks of the

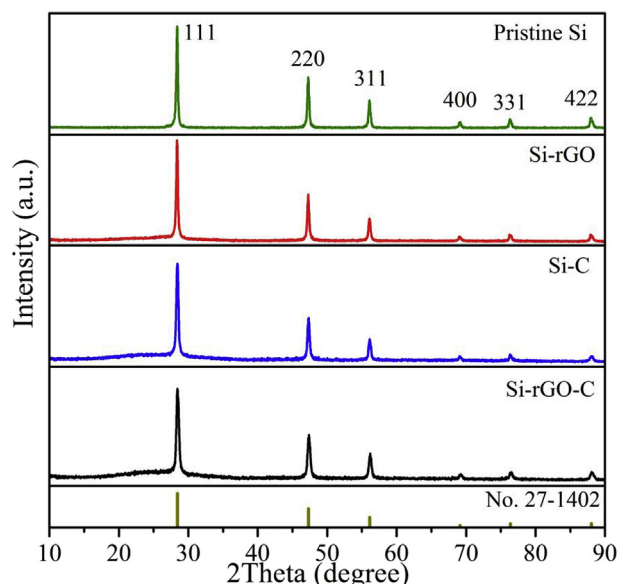


Fig. 2. XRD patterns of pristine Si, Si-rGO, Si-C and Si-rGO-C samples.

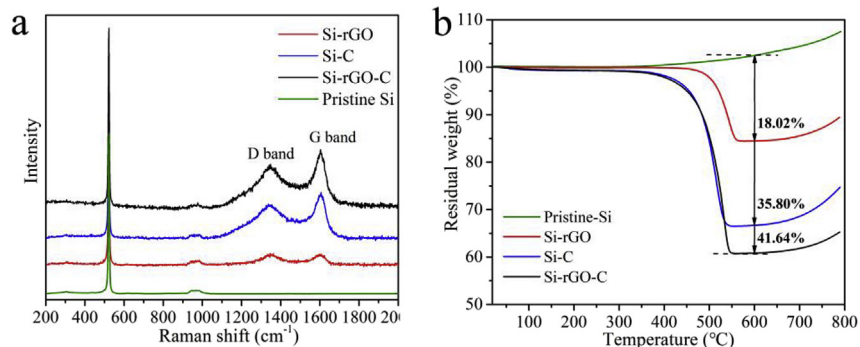


Fig. 3. Raman spectra and TG curves of pristine Si, Si-rGO, Si-C and Si-rGO-C samples.

synthesized Si-rGO, Si-C and Si-rGO-C composites match well with pristine Si and agree with the (111), (220), (311), (400), (331), and (422) diffraction planes of cubic structure Si (JCDPF card No. 27-1402).

For the Raman spectra of all four samples (Fig. 3a), a strong peak located at 521 cm^{-1} and a small peak at 954 cm^{-1} should correspond to the characteristic Raman shift of crystalline Si [37–39]. The broad peaks at 1346 and 1600 cm^{-1} in Si-rGO, Si-C and Si-rGO-C composites correspond to D and G bands of the carbon (amorphous carbon and rGO), which are linked to disordered carbon and relative motion of sp^2 -bonded graphitic carbon atoms, respectively

[40–42]. The results indicate that carbon materials have been successfully introduced into the composites. The TG curves of these samples are shown in Fig. 3b. All samples are heated to 800 $^{\circ}\text{C}$ in air so that Si is partly oxidized to SiO_x and carbon is combusted to CO_2 [43,44]. The weight loss of three composites between 400 and 600 $^{\circ}\text{C}$ should be attributed to these two processes together. The residual weight of pristine Si is about 102.49%, thus the carbon contents of Si-rGO, Si-C and Si-rGO-C composites are determined to be 18.02%, 35.80% and 41.64%, respectively.

The SEM images of Si-rGO, Si-C and Si-rGO-C composites are presented in Fig. 4. The three composites show distinctly different

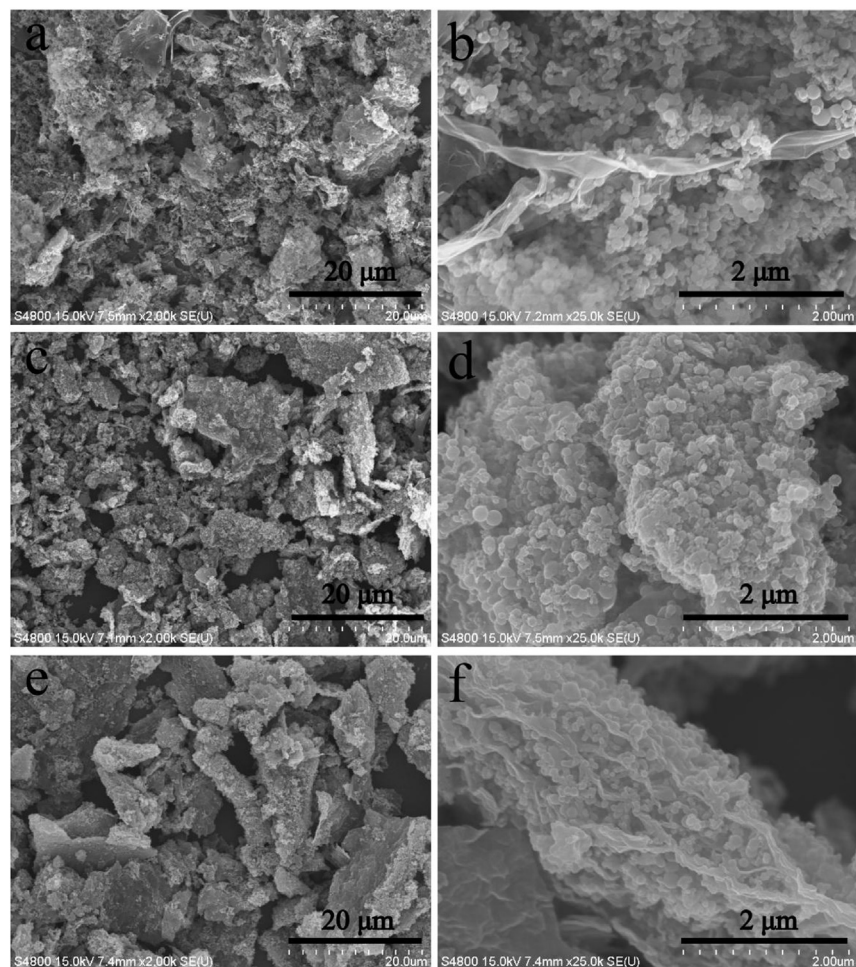


Fig. 4. SEM images of (a, b) Si-rGO composite, (c, d) Si-C composite and (e, f) Si-rGO-C composite.

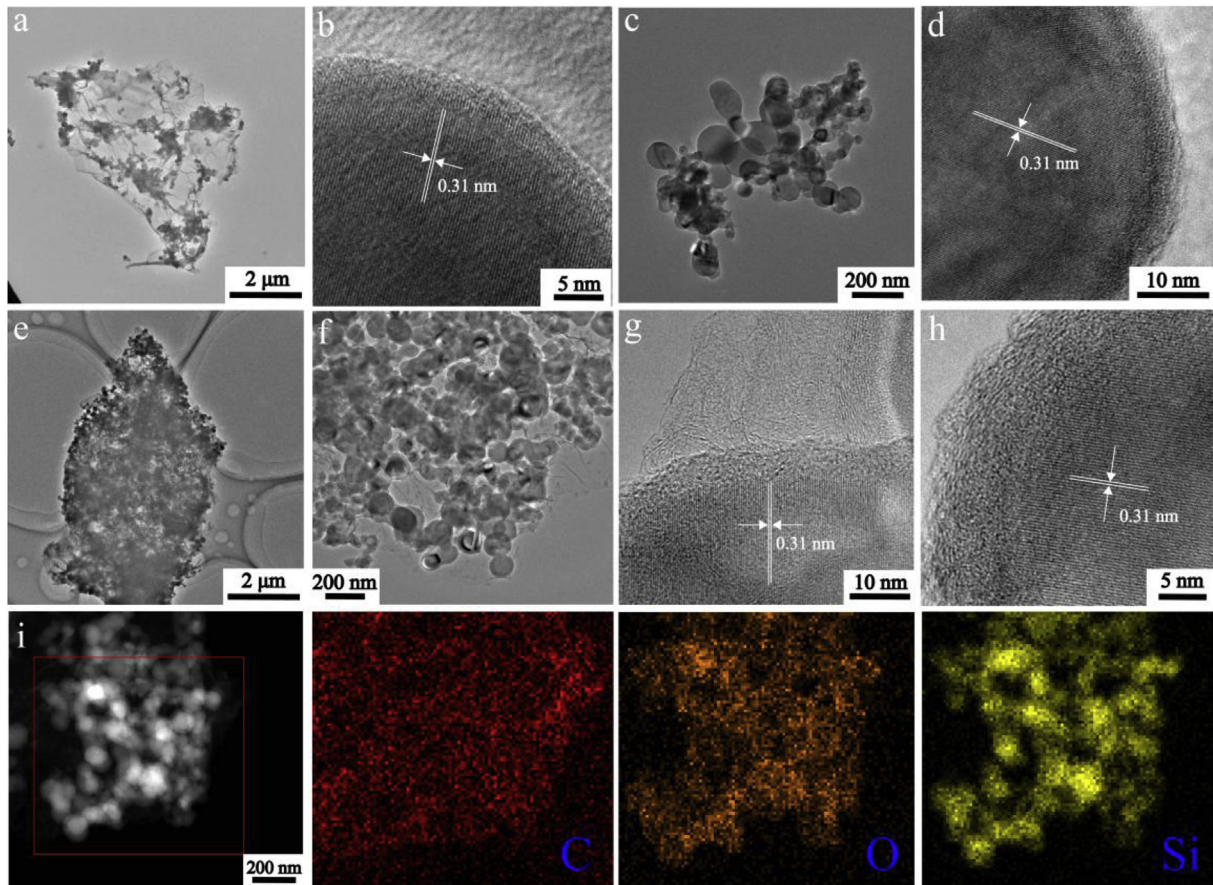


Fig. 5. TEM images of (a, b) Si-rGO composite, (c, d) Si-C composite and (e, f, g, h) Si-rGO-C composite. (i) HAADF image and corresponding elemental mapping of Si-rGO-C composite.

morphologies. We can see wrinkled rGO sheets in the Si-rGO composite (Fig. 4a and b). However, the contact between Si NPs and rGO is very loose without guar gum serving as the “glue”. For the Si-C composite (Fig. 4c and d), Si NPs are encapsulated by amorphous carbon and interconnected to micro scale clusters due to the carbonization of guar gum hydrogel. The Si-rGO-C composite (Fig. 4e) looks like a pile of books scattered on the floor. In every “book”, Si NPs are interconnected to clusters by amorphous carbon like Si-C composite and well wrapped by rGO sheets (Fig. 4f).

The TEM images of these composites are shown in Fig. 5. After ultrasonic treatment which is used to disperse samples prior to TEM characterization, there is only a little amount of Si NPs still anchored on the rGO sheets for the Si-rGO composite (Fig. 5a). However, the bonding between Si NPs and rGO in the Si-rGO-C composite is very strong (Fig. 5e). In Fig. 5b, an amorphous layer (SiO_x) of about 2 nm in thickness can be observed on the surface of a single Si NP. The lattice fringes inside are calibrated to have a lattice spacing of $d = 0.31 \text{ nm}$, corresponding to the (111) plane of crystalline Si. Fig. 5d reveals that the amorphous carbon layer (about 7 nm in thickness) has been coated onto Si NPs in the Si-C composite. Fig. 5e and f reveal that Si NPs are interconnected and tightly anchored to the rGO in the Si-rGO-C composite. Double coating layers made of amorphous carbon and rGO (wrinkles in Fig. 5g and h) can be clearly observed on the surface of Si NPs. The EDX mapping was also conducted on the Si-rGO-C composite (Fig. 5i). Si and O elements are homogenously distributed in the C element, suggesting that Si NPs are uniformly spread in the carbon matrix consist of rGO and amorphous carbon.

To investigate the enhanced electronic conductivity of these composites induced by the introduction of carbon materials, powder electronic conductivity of pristine Si, Si-rGO, Si-C and Si-rGO-C samples were measured at the pressure of 2 MPa. As shown in Table 1, the hybridization with both amorphous carbon and graphene can effectively increase the electronic conductivity of Si-based materials. And the Si-rGO-C composite possesses the highest electronic conductivity. Thus constructing synergistic carbon coating layers is very important in the Si-rGO-C composite. The carbon coating layer can enhance the electronic conductivity of Si NPs and help to form stable solid electrolyte interface (SEI) on the surface. The highly conductive and flexible rGO can further facilitate electrons transport through the whole electrode and accommodate huge volume changes during cycling. The Si-rGO-C composite is expected to possess superior electrochemical performance benefit by the synergistic carbon coating layers in the composite structure.

Fig. 6 presents the CV curves of the Si-rGO-C composite at the scan rate of 0.1 mV s^{-1} between 0.02 and 1.5 V vs Li^+/Li . For the first

Table 1
Powder electronic conductivity of pristine Si, Si-rGO, Si-C and Si-rGO-C samples measured at the pressure of 2 MPa.

Samples	Conductivity (S cm^{-1})
Pristine Si	7.58×10^{-6}
Si-rGO composite	1.18
Si-C composite	0.059
Si-rGO-C composite	2.91

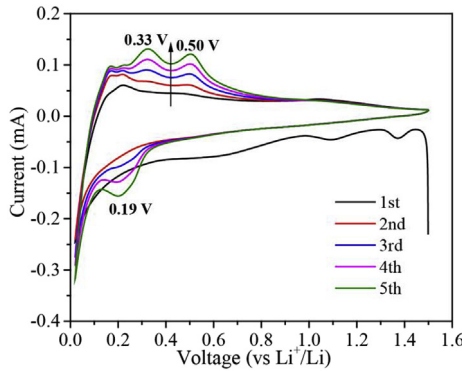


Fig. 6. Cyclic voltammetry (CV) curves of the Si-rGO-C composite for the first 5 cycles at the scan rate of 0.1 mV s^{-1} between 0.02 and 1.5 V vs Li^+/Li .

cathodic process, two broad peaks at around 1.37 and 1.12 V can be attributed to the side reactions of Li^+ ions with the residual oxygen-containing groups in rGO and the formation of solid electrolyte

layer (SEI), which disappear in the following cycles [33,45]. The two weak anodic peaks at 0.15–0.2 V may be due to the reaction of Li^+ with carbon materials (rGO and amorphous carbon) [46–48]. The cathodic peak at ~0.19 V and the anodic peaks at ~0.33 and ~0.50 V are characteristic peaks of amorphous Si, and the cathodic peak at nearly 0 V is coincidental for both crystalline and amorphous Si [47,49]. Because Si in the Si-rGO-C composite is crystalline, only one peak at ~0 V is observed in the first cathodic process. An additional cathodic peak at ~0.19 V appears in the cathodic processes, and two anodic peaks at ~0.33 and ~0.50 V which are related to the dealloy steps of Li_xSi become broader and stronger as a result of cycling [50,51]. This phenomenon is a common feature to the conversion of crystalline Si into amorphous Si during the repeated lithiation and delithiation [16,52,53].

The electrochemical performances of Si-rGO, Si-C and Si-rGO-C composites are evaluated by the galvanostatic method. The cyclic performances of these samples at 0.5 A g^{-1} are shown in Fig. 7a. These electrodes were activated at 0.1 A g^{-1} for the first 5 cycles and then cycled at the higher current densities for all the subsequent cycles. Obviously, the Si-rGO-C composite exhibits the best cyclic stability. The first charge capacity of the Si-rGO-C composite at 0.5 A g^{-1} (the

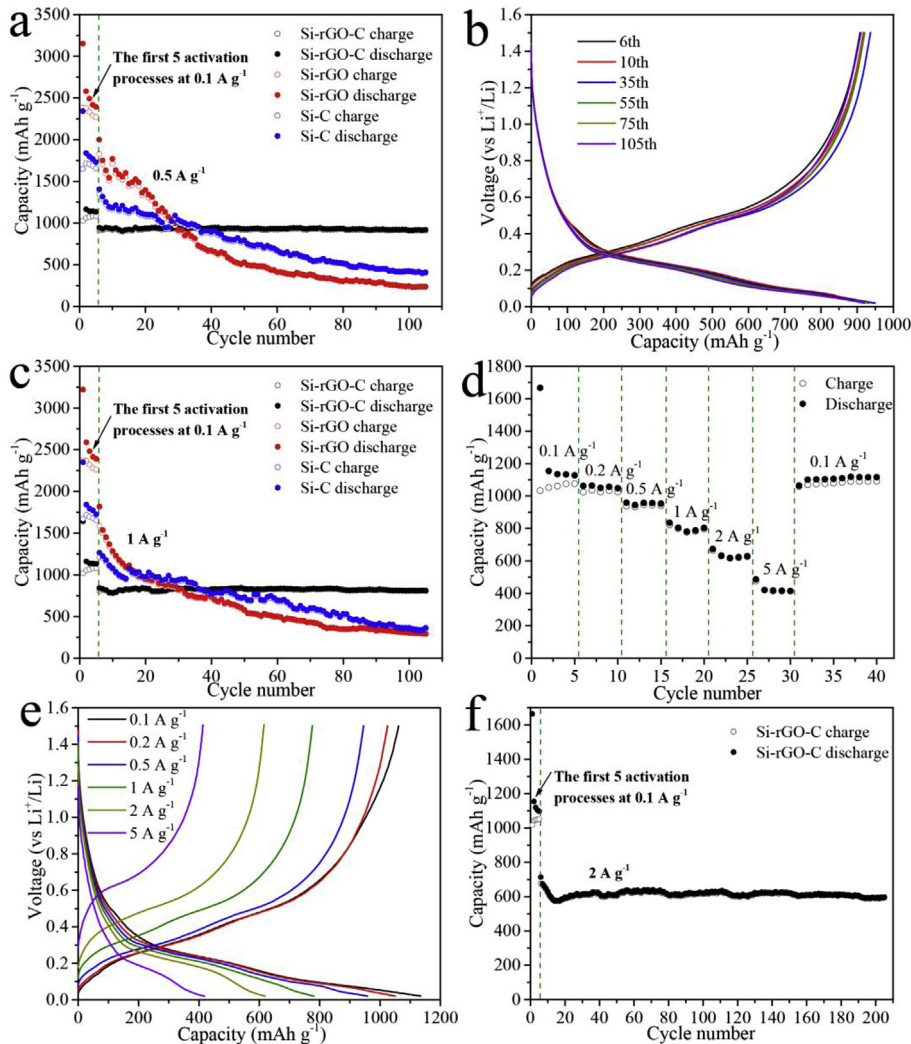


Fig. 7. (a) Cyclic performances of Si-rGO, Si-C and Si-rGO-C composites at the current density of 0.5 A g^{-1} . (b) Typical charge-discharge voltage profiles of the Si-rGO-C composite at the current density of 0.5 A g^{-1} . (c) Cyclic performances of Si-rGO, Si-C and Si-rGO-C composites at the current density of 1 A g^{-1} . (d) Rate performances and (e) charge-discharge voltage profiles of the Si-rGO-C composite at the current densities from 0.1 A g^{-1} to 5 A g^{-1} . (f) Long-term cyclic performances of the Si-rGO-C composite at the current density of 2 A g^{-1} .

6th cycle) is 913 mAh g^{-1} . And the high capacity of 910 mAh g^{-1} is still retained after 100 cycles, which indicates a negligible capacity decay. The charge-discharge voltage profiles of the Si-rGO-C composite (Fig. 7b) overlap well during cycling, which reflects the high cyclic stability and small polarization degree of the electrode. The Si-rGO and Si-C composites show higher initial charge capacities (1829 and 1348 mAh g^{-1} , respectively) at 0.5 A g^{-1} , due to the higher content of Si in the composites. However, the capacities fade quickly after 100 cycles corresponding to the charge capacity retention of 13% and 30% , respectively. At a higher current density of 1 A g^{-1} , the Si-rGO-C composite shows a charge capacity of 805 mAh g^{-1} , with a charge capacity retention of 98.3% . However, the Si-rGO and Si-C composites only exhibit charge capacities of 291 and 354 mAh g^{-1} with charge capacity retentions of 18% and 29% , respectively.

Rate capability of the Si-rGO-C composite was also investigated (Fig. 7d and e). The cells were cycled at various current densities ranging from 0.1 A g^{-1} to 5 A g^{-1} . The Si-rGO-C composite exhibits an average capacity of 1060 mAh g^{-1} at the low current density of 0.1 A g^{-1} . The reversible capacities of 1029 , 940 , 795 and 632 mAh g^{-1} can be achieved at the high current densities of 0.2 , 0.5 , 1 and 2 A g^{-1} , respectively. Even at a very high current density of 5 A g^{-1} (every cycle finished at about 10 min), a high reversible capacity of 428 mAh g^{-1} is maintained which is still higher than the theoretical capacity of graphite. Besides, after the current density returns to 0.1 A g^{-1} , the charge capacity quickly recovers to 1059 mAh g^{-1} , which demonstrates the good reversibility. The long-term cyclic performance is another important character to LIB anodes. The Si-rGO-C composite exhibits the charge capacity of 593 mAh g^{-1} with the capacity retention of 88% after 200 cycles at the high current density of 2 A g^{-1} (Fig. 7f), demonstrating the outstanding long-term cyclic stability during high rate cycling.

To further study the origin of the superior electrochemical performance, EIS measurements of all the composites electrodes were performed after the initial cycle at the fully delithiated state. Every EIS plot consists of a compressed semicircle in the high to medium frequency region and a straight line in the low frequency region (Fig. 8). The semicircle is attributed to the charge-transfer resistance (R_{ct} , might contain the SEI film resistance and the inter-particle contact resistance), and the incline line is related to the diffusion of Li^+ ions into the anode material [54,55]. The EIS data are fitted by using the equivalent circuit (inset in Fig. 8), and more details are shown in Table 2. These results clearly reveal that the Si-rGO-C composite electrode presents the smallest R_{ct} among

Table 2

Equivalent-circuit parameters and errors obtained from fitting the experimental impedance spectra.

Sample	$R_{ele} (\Omega)$	Error (%)	$R_{ct} (\Omega)$	Error (%)
Si-rGO	3.276	2.53	39.05	1.38
Si-C	5.195	1.53	29.76	1.28
Si-rGO-C	2.823	2.21	22.57	1.38

all the three samples, which is favorable for rapid charge and discharge.

Among the three composites studied, the Si-rGO-C composite possesses the best electrochemical performance. The superior cyclic stability can be attributed to the successful construction of the synergistic protective layers (amorphous carbon and rGO). The Si-rGO and Si-C composites with a singular protective layer can not ensure the structural integrity and electronic conductivity in the whole electrode.

4. Conclusions

The Si-rGO-C ternary composite with synergistic protective layers of both amorphous carbon and rGO has been successfully synthesized by a facile guar gel hydrogel method. The amorphous carbon and rGO serve as synergistic protective layers. The amorphous carbon coating layer embedded with Si NPs can enhance electronic conductivity and help to form the stable SEI layers on the surface. The rGO coating layers not only form a conductive network in the whole material but also can buffer the mechanical stress induced by volume change of Si during cycling. Thus the excellent structural stability and conductive network offer the Si-rGO-C ternary composite superior electrochemical performance, compared with the Si-rGO and Si-C composites with a singular protective layer. Besides, all the raw materials are commercial products and the synthesis route is simple and scalable. The Si-rGO-C ternary composite can be a promising high capacity anode for LIBs.

Acknowledgements

The authors gratefully acknowledge financial support from National Natural Science Foundation of China (21273185 and 21321062) and Key Project of Science and Technology of Xiamen (3502Z20141008). The authors also wish to express their thanks to Prof. Daiwei Liao of Xiamen University for his valuable discussion and suggestion.

References

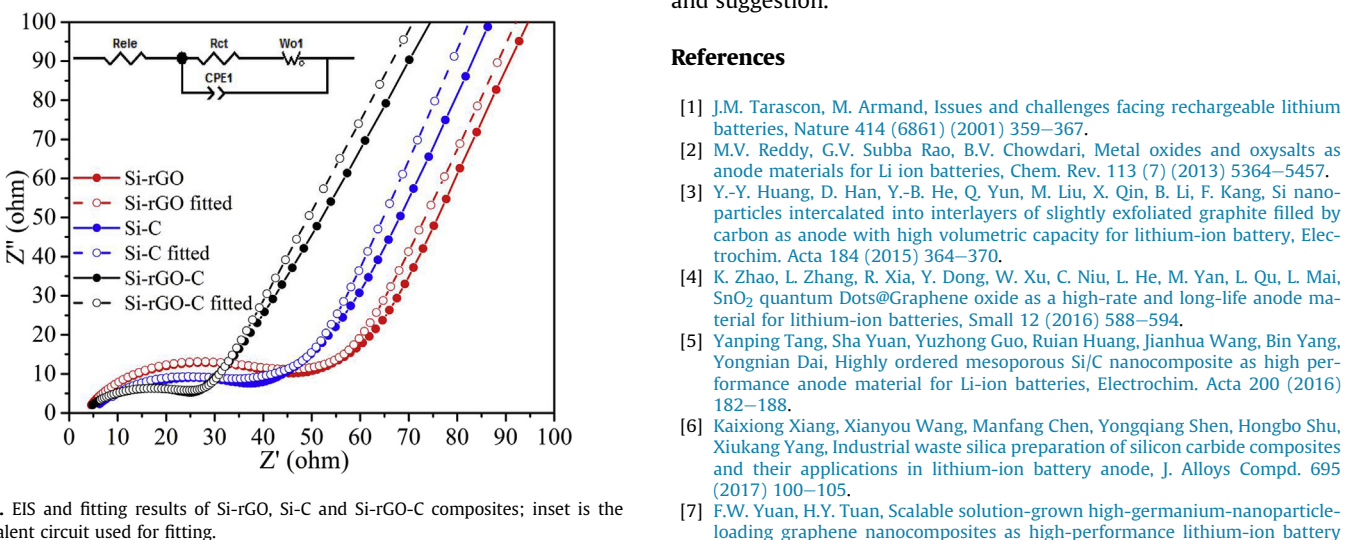


Fig. 8. EIS and fitting results of Si-rGO, Si-C and Si-rGO-C composites; inset is the equivalent circuit used for fitting.

- [1] J.M. Tarascon, M. Armand, Issues and challenges facing rechargeable lithium batteries, *Nature* 414 (6861) (2001) 359–367.
- [2] M.V. Reddy, G.V. Subba Rao, B.V. Chowdari, Metal oxides and oxy salts as anode materials for Li ion batteries, *Chem. Rev.* 113 (7) (2013) 5364–5457.
- [3] Y.-Y. Huang, D. Han, Y.-B. He, Q. Yun, M. Liu, X. Qin, B. Li, F. Kang, Si nanoparticles intercalated into interlayers of slightly exfoliated graphite filled by carbon as anode with high volumetric capacity for lithium-ion battery, *Electrochim. Acta* 184 (2015) 364–370.
- [4] K. Zhao, L. Zhang, R. Xia, Y. Dong, W. Xu, C. Niu, L. He, M. Yan, L. Qu, L. Mai, SnO_2 quantum dots@Graphene oxide as a high-rate and long-life anode material for lithium-ion batteries, *Small* 12 (2016) 588–594.
- [5] Yanping Tang, Sha Yuan, Yuzhong Guo, Ruian Huang, Jianhua Wang, Bin Yang, Yongnian Dai, Highly ordered mesoporous Si/C nanocomposite as high performance anode material for Li-ion batteries, *Electrochim. Acta* 200 (2016) 182–188.
- [6] Kaixiong Xiang, Xianyou Wang, Manfang Chen, Yongqiang Shen, Hongbo Shu, Xiukang Yang, Industrial waste silica preparation of silicon carbide composites and their applications in lithium-ion battery anode, *J. Alloys Compd.* 695 (2017) 100–105.
- [7] F.W. Yuan, H.Y. Tuan, Scalable solution-grown high-germanium-nanoparticle-loading graphene nanocomposites as high-performance lithium-ion battery

- electrodes: an example of a graphene-based platform toward practical full-cell applications, *Chem. Mater.* 26 (2014) 2172–2179.
- [8] H. Wu, G. Zheng, N. Liu, T.J. Carney, Y. Yang, Y. Cui, Engineering empty space between Si nanoparticles for lithium-ion battery anodes, *Nano Lett.* 12 (2) (2012) 904–909.
- [9] M. Shimizu, H. Usui, K. Matsumoto, T. Nokami, T. Itoh, H. Sakaguchi, Effect of cation structure of ionic liquids on anode properties of Si electrodes for LIB, *J. Electrochim. Soc.* 161 (2014) A1765–A1771.
- [10] Masakazu Haruta, Takashi Okubo, Yuta Masuo, Shuhei Yoshida, Akira Tomita, Toshio Takenaka, Takayuki Doi, Minoru Inaba, Temperature effects on SEI formation and cyclability of Si nanoflake powder anode in the presence of SEI-forming additives, *Electrochim. Acta* 224 (2017) 186–193, <http://dx.doi.org/10.1016/j.electacta.2016.12.071>.
- [11] Shilong Jing, Hao Jiang, Yanjie Hu, Jianhua Shen, Chunzhong Li, Face-to-Face contact and open-void coinvolved Si/C nanohybrids lithium-ion battery anodes with extremely long cycle life, *Adv. Funct. Mater.* 25 (33) (2015) 5395–5401.
- [12] Rong Zhou, Huajun Guo, Yong Yang, Zhixing Wang, Xinhai Li, Yu Zhou, N-doped carbon layer derived from polydopamine to improve the electrochemical performance of spray-dried Si/graphite composite anode material for lithium ion batteries, *J. Alloys Compd.* 689 (2016) 130–137.
- [13] L. Sun, T. Su, L. Xu, H.B. Du, Preparation of uniform Si nanoparticles for high-performance Li-ion battery anodes, *Phys. Chem. Chem. Phys.* PCCP 18 (3) (2016) 1521–1525.
- [14] Claude Hoeltgen, Jeong-Eun Lee, Bo-Yun Jang, Stepwise carbon growth on Si/SiO_x core-shell nanoparticles and its effects on the microstructures and electrochemical properties for high-performance lithium-ion battery's anode, *Electrochim. Acta* 222 (2016) 535–542.
- [15] B. Salhi, M.K. Hossain, A.W. Mukhaimer, F.A. Al-Sulaiman, Nanowires: a new pathway to nanotechnology-based applications, *J. Electroceram.* 37 (1–4) (2016) 34–49.
- [16] M. Ge, J. Rong, X. Fang, C. Zhou, Porous doped silicon nanowires for lithium ion battery anode with long cycle life, *Nano Lett.* 12 (5) (2012) 2318–2323.
- [17] R.V. Salvatierra, A.R.O. Raji, S.K. Lee, Y.S. Ji, L. Li, J.M. Tour, Silicon nanowires and lithium cobalt oxide nanowires in graphene nanoribbon papers for full lithium ion battery, *Adv. Energy Mater.* 6 (2016).
- [18] T. Song, J. Xia, J.H. Lee, D.H. Lee, M.S. Kwon, J.M. Choi, J. Wu, S.K. Doo, H. Chang, W.I. Park, D.S. Zang, H. Kim, Y. Huang, K.C. Hwang, J.A. Rogers, U. Paik, Arrays of sealed silicon nanotubes as anodes for lithium ion batteries, *Nano Lett.* 10 (5) (2010) 1710–1716.
- [19] Bharat Gattu, Rigved Epur, Prashanth H. Jampani, Ramalinga Kuruba, Moni Kanchan Datta, Prashant N. Kumta, Silicon–carbon core–shell hollow nanotubular configuration high-performance lithium-ion anodes, *J. Phys. Chem. C* 121 (18) (2017) 9662–9671.
- [20] M.T. Demirkan, L. Trahey, T. Karabacak, Low-density silicon thin films for lithium-ion battery anodes, *Thin Solid Films* 600 (2016) 126–130.
- [21] D.S.M. Iaboni, M.N. Obrovac, Li₁₅Si₄ formation in silicon thin film negative electrodes, *J. Electrochim. Soc.* 163 (2016) A255–A261.
- [22] Z.W. Zhou, Y.T. Liu, X.M. Xie, X.Y. Ye, Constructing novel Si@SnO₂ core–shell heterostructures by facile self-assembly of SnO₂ nanowires on silicon hollow nanospheres for large, reversible lithium storage, *ACS Appl. Mater. Interfaces* 8 (2016) 7092–7100.
- [23] Z.W. Zhou, Y.T. Liu, X.M. Xie, X.Y. Ye, Aluminothermic reduction enabled synthesis of silicon hollow microspheres from commercialized silica nanoparticles for superior lithium storage, *Chem. Commun.* 52 (2016) 8401–8404.
- [24] A. Bhownik, R. Malik, S. Prakash, T. Sarkar, M.D. Bharadwaj, S. Aich, S. Ghosh, Classical molecular dynamics and quantum ab-initio studies on lithium-intercalation in interconnected hollow spherical nano-spheres of amorphous silicon, *J. Alloys Compd.* 665 (2016) 165–172.
- [25] Jeannine R. Szczech, Song Jin, Nanostructured silicon for high capacity lithium battery anodes, *Energy Environ. Sci.* 4 (1) (2011) 56–72.
- [26] Xin Su, Qingliu Wu, Juchuan Li, Xingcheng Xiao, Amber Lott, Wenquan Lu, Brian W. Sheldon, Ji Wu, Silicon-based nanomaterials for lithium-ion batteries: a review, *Adv. Energy Mater.* 4 (1) (2014) 1300882.
- [27] Zailei Zhang, Yanhong Wang, Wenfeng Ren, Qiangqiang Tan, Yunfa Chen, Hong Li, Ziyi Zhong, Fabing Su, Scalable synthesis of interconnected porous silicon/carbon composites by the rochow reaction as high-performance anodes of lithium ion batteries, *Angew. Chem.* 126 (20) (2014) 5265–5269.
- [28] W.H. Zhang, X.Y. Chen, T.Q. Yong, N. Xu, R.F. Guan, L. Yue, Multiwalled carbon nanotube webs welded with Si nanoparticles as high-performance anode for lithium-ion batteries, *J. Alloys Compd.* 688 (2016) 216–224.
- [29] Dingqiong Chen, Wenjuan Liao, Yang Yang, Jinbao Zhao, Polyvinyl alcohol gelation: a structural locking-up agent and carbon source for Si/CNT/C composites as high energy lithium ion battery anode, *J. Power Sources* 315 (2016) 236–241.
- [30] Quan Xu, Jin-Yi Li, Jian-Kun Sun, Ya-Xia Yin, Li-Jun Wan, Yu-Guo Guo, Watermelon-inspired Si/C microspheres with hierarchical buffer structures for densely compacted lithium-ion battery anodes, *Adv. Energy Mater.* 7 (3) (2017) 1601481.
- [31] Xiaosi Zhou, Ya-Xia Yin, Li-Jun Wan, Yu-Guo Guo, Self-assembled nanocomposite of silicon nanoparticles encapsulated in graphene through electrostatic attraction for lithium-ion batteries, *Adv. Energy Mater.* 2 (9) (2012) 1086–1090.
- [32] Xiongwu Zhong, Zhenzhong Yang, Xiaowu Liu, Jiaqing Wang, Lin Gu, Yan Yu, General strategy for fabricating sandwich-like graphene-based hybrid films for highly reversible lithium storage, *ACS Appl. Mater. Interfaces* 7 (33) (2015) 18320–18326.
- [33] N. Lin, J. Zhou, L. Wang, Y. Zhu, Y. Qian, Polyaniline-assisted synthesis of Si/C/RGO as anode material for rechargeable lithium-ion batteries, *ACS Appl. Mater. Interfaces* 7 (2015) 409–414.
- [34] Jingbo Chang, Xingkang Huang, Guihua Zhou, Shumao Cui, Shun Mao, Junhong Chen, Three-dimensional carbon-coated Si/RGO nanostructures anchored by nickel foam with carbon nanotubes for Li-ion battery applications, *Nano Energy* 15 (2015) 679–687.
- [35] M.-H. Lin, S. Hy, C.-Y. Chen, J.-H. Cheng, J. Rick, N.-W. Pu, W.-N. Su, Y.-C. Lee, B.-J. Hwang, Resilient yolk-shell silicon-reduced graphene oxide/amorphous carbon anode material from a synergistic dual-coating process for lithium-ion batteries, *ChemElectroChem* 3 (2016) 1446–1454.
- [36] Manoj K. Jangid, Farjana J. Sonia, Ravi Kali, Balakrishna Ananthouju, Amartya Mukhopadhyay, Insights into the effects of multi-layered graphene as buffer/interlayer for a-Si during lithiation/delithiation, *Carbon* 111 (2017) 602–616.
- [37] T.A. Harriman, D.A. Lucca, J.-K. Lee, M.J. Klopstein, K. Herrmann, M. Nastasi, Ion implantation effects in single crystal Si investigated by Raman spectroscopy, *Nucl. Instrum. Methods Phys. Res. Sect. B Beam Interact. Mater. Atoms* 267 (8–9) (2009) 1232–1234.
- [38] Yang Yang, Jiaqi Li, Dingqiong Chen, Tao Fu, Dong Sun, Jinbao Zhao, Binder-Free carbon-coated silicon-reduced graphene oxide nanocomposite electrode prepared by electrokinetic deposition as a high-performance anode for lithium-ion batteries, *ChemElectroChem* 3 (5) (2016) 757–763.
- [39] José Menéndez, Manuel Cardona, Temperature dependence of the first-order Raman scattering by phonons in Si, Ge, and α -Sn: anharmonic effects, *Phys. Rev. B* 29 (4) (1984) 2051–2059.
- [40] R. Sun, Q. Wei, Q. Li, W. Luo, Q. An, J. Sheng, D. Wang, W. Chen, L. Mai, Vanadium sulfide on reduced graphene oxide layer as a promising anode for sodium ion battery, *ACS Appl. Mater. Interfaces* 7 (37) (2015) 20902–20908.
- [41] Jiarui He, Yuanfu Chen, Weiqiang Lv, Kechun Wen, Zegao Wang, Wanli Zhang, Yanrong Li, Wu Qin, Weidong He, Three-Dimensional hierarchical reduced graphene oxide/tellurium nanowires: a high-performance freestanding cathode for Li–Te batteries, *ACS Nano* 10 (9) (2016) 8837–8842.
- [42] Yonghai Song, Li Zuo, Shouhui Chen, Jiafeng Wu, Haoqing Hou, Li Wang, Porous nano-Si/carbon derived from zeolitic imidazolate Frameworks@Nano-Si as anode materials for lithium-ion batteries, *Electrochim. Acta* 173 (2015) 588–594.
- [43] X.Y. Zhu, H. Chen, Y.H. Wang, L.H. Xia, Q.Q. Tan, H. Li, Z.Y. Zhong, F.B. Su, X.S. Zhao, Growth of silicon/carbon microrods on graphite microspheres as improved anodes for lithium-ion batteries, *J. Mater. Chem. A* 1 (2013) 4483–4489.
- [44] J.L. Yu, J. Yang, X.J. Feng, H. Jia, J.L. Wang, W. Lu, Uniform carbon coating on silicon nanoparticles by dynamic CVD process for electrochemical lithium storage, *Ind. Eng. Chem. Res.* 53 (2014) 12697–12704.
- [45] H. Tang, J.-p. Tu, X.-y. Liu, Y.-j. Zhang, S. Huang, W.-z. Li, X.-l. Wang, C.-d. Gu, Self-assembly of Si/honeycomb reduced graphene oxide composite film as a binder-free and flexible anode for Li-ion batteries, *J. Mater. Chem. A* 2 (2014) 5834–5840.
- [46] K.A. Striebel, A. Sierra, J. Shim, C.-W. Wang, A.M. Sastry, The effect of compression on natural graphite anode performance and matrix conductivity, *J. Power Sources* 134 (2) (2004) 241–251.
- [47] X. Chen, X. Li, F. Ding, W. Xu, J. Xiao, Y. Cao, P. Meduri, J. Liu, G.L. Graff, J.G. Zhang, Conductive rigid skeleton supported silicon as high-performance Li-ion battery anodes, *Nano Lett.* 12 (8) (2012) 4124–4130.
- [48] R. Hu, W. Sun, Y. Chen, M. Zeng, M. Zhu, Silicon/graphene based nanocomposite anode: large-scale production and stable high capacity for lithium ion batteries, *J. Mater. Chem. A* 2 (2014) 9118–9125.
- [49] M.N. Obrovac, L.J. Krause, Reversible cycling of crystalline silicon powder, *J. Electrochim. Soc.* 154 (2007) A103–A108.
- [50] Xiuyan Wang, Zhaoxin Wen, Yu Liu, Xiaogang Xu, Jiu Lin, Preparation and characterization of a new nanosized silicon–nickel–graphite composite as anode material for lithium ion batteries, *J. Power Sources* 189 (1) (2009) 121–126.
- [51] Shuangqiang Chen, Laifa Shen, Peter A. van Aken, Joachim Maier, Yan Yu, Dual-functionalized double carbon shells coated silicon nanoparticles for high performance lithium-ion batteries, *Adv. Mater.* 29 (21) (2017) 1605650.
- [52] F.M. Hassan, V. Chabot, A.R. Elsayed, X. Xiao, Z. Chen, Engineered Si electrode nanoarchitecture: a scalable postfabrication treatment for the production of next-generation Li-ion batteries, *Nano Lett.* 14 (1) (2014) 277–283.
- [53] Huajun Tian, Xiaoqian Tan, Fengxia Xin, Chunsheng Wang, Weiqiang Han, Micro-sized nano-porous Si/C anodes for lithium ion batteries, *Nano Energy* 11 (2015) 490–499.
- [54] X. Liu, Q. Su, C. Zhang, T. Huang, A. Yu, Enhanced electrochemical performance of Li_{1.2}Mn_{0.54}Ni_{0.13}Co_{0.13}O₂ cathode with an ionic conductive LiVO₃ coating layer, *ACS Sustain. Chem. Eng.* 4 (2016) 255–263.
- [55] L. Cheng, X.-L. Li, H.-J. Liu, H.-M. Xiong, P.-W. Zhang, Y.-Y. Xia, Carbon-coated Li₄Ti₅O₁₂ as a high rate electrode material for Li-ion intercalation, *J. Electrochim. Soc.* 154 (2007) A692–A697.